A space vector PWM algorithm for a three-level asymmetrical six-phase motor drive

Engku Ahmad Rafiqi Bin Engku Ariff [1], Obrad Dordevic [2*], Martin Jones [2]

[1] School of Electrical System Engineering, Universiti Malaysia Perlis, Pauh Putra Campus, 02600 Arau, Perlis, Malaysia
[2] Department of Electronics and Electrical Engineering, Liverpool John Moores University, James Parsons Building L3 3AF, Liverpool, U.K.
[*]O.Dordevic@ljmu.ac.uk

Abstract: A space vector pulse-width modulation (SVPWM) algorithm for a three-level asymmetrical six-phase drive based on vector space decomposition (VSD) approach is presented in this paper. A modification in zero plane of the transformation matrix is proposed in order to meet the requirement that the realisation of sinusoidal output phase voltages can be obtained through the chosen output leg voltage space vectors. Furthermore, a method of choosing the switching sequences based on all possible one-level transitions of the leg voltages, i.e. a permutation method, is introduced. The algorithm is then validated experimentally and obtained results show that the developed method successfully achieves the desired fundamental phase voltage, although low order harmonics are present due to uncompensated inverter dead time. Last but not least, the performance of the proposed SVPWM algorithm is compared to several carrier-based PWM algorithms including in-phase disposition with 'double min-max injection' (PD-DI). This is a little-known type of injection, which is verified to obtain identical performance as the presented multilevel algorithm.

1. Introduction

The advantages offered by multiphase drives, when compared to the already matured technology of three-phase drives, are well known and understood at this point in time [1]. The main advantage of a multiphase drive is that it offers greater fault tolerance capabilities compared to the conventional three-phase drives. If a fault takes place in one of the three-phase machine's stator windings, the machine becomes single-phase and is not able to properly operate any more. However, this is not the case for multiphase machines, as investigated in [2] for six-phase drives. As a result, the research developments done in the area of multiphase drives have progressed significantly in recent years and more and more attention is given to multiphase drives with multiple three-phase winding sets, such as six- or nine-phase machines [3, 4]. This is so since, by simply rewinding the stator of the widely available three-phase machines, this type of multiphase machines can be constructed, hence enabling a saving in the manufacturing cost.

A multiphase drive refers to a multiphase machine together with its corresponding multiphase inverter. The higher number of machine's phases allows the current flowing form the dc-bus to be shared between the phases thus giving more flexibility of choosing power semiconductors, with much lower rating, when designing an inverter. In addition, the topology of the inverter used to drive the multiphase machine is not only restricted to the conventional two-level structure. Multilevel structures, such as the neutral point clamped (NPC) topology introduced in [5], can be used as well. Furthermore, by adding multilevel inverter's ability to sustain much higher dc-bus voltage, on top of the possibility of using much lower rating for power semiconductors, a much higher power drive can be realised. However, from the control point of view, as the number of the inverter output leg voltage levels and the number of the machine phases increase, the complexity of developing proper PWM techniques also increases, especially for the SVPWM case. Yet, as shown later, all the complex steps required for developing the SVPWM algorithm can be done offline, thus keeping the implementation of the algorithm fairly simple.

Among the carrier-based PWM techniques available for multilevel inverters, it has been shown that in-phase disposition PWM (PD-PWM) has the lowest voltage harmonic distortion [6]. In addition, it has also been shown in [7-9] that by using PD-PWM and injecting twice zero sequence into reference voltage waveforms (referred henceforth as 'double min-max injection' in this paper, i.e. PD-DI), similar results as with SVPWM technique can be obtained. However, unlike PD-DI, which can easily be extended to any number of inverter's voltage levels and machine's phases, the SVPWM algorithm is unique to the drive topology it has been developed for, hence the complexity. The first successful SVPWM algorithm for multilevel multiphase drive was presented in [10]. The developed algorithm is based on VSD approach, introduced in [11], and is intended for a five-phase machine driven by a three-level NPC inverter. Further, for the same drive topology, the algorithm has been improved further with the aim of reducing the variation in common mode voltage (CMV) in [12]. Moreover, based on the approaches presented in the improved algorithm, two SVPWM algorithms are later successfully developed and presented in [13] and [14] for three-level symmetrical six-phase and seven-phase drives, respectively. Furthermore, a performance comparison between PD-DI and SVPWM algorithm is also reported in [12-14], where their performances are proven to be identical for all three drive topologies.

In this paper, a novel SVPWM algorithm based on VSD approach is developed and experimentally validated for a three-level asymmetrical six-phase drive, with a single

isolated neutral point. The importance of developing new SVPWM algorithms for multiphase multilevel drives cannot be overstated. The deeper understanding of these algorithms can lead to significant insights pointing the way to further developments in fault tolerant control, model predictive control and low switching frequency modulations for high power applications. These insights are not possible from the carrier-based modulation perspective.

One of the main practical issues related to NPC topology is the dc-link capacitors voltage balancing. Typically, voltage balancing methods, which are based on software solutions, use common mode voltage injection [15] or multi-step operation of the converter [16]. However, the focus in this paper is on the algorithm development and the voltage balancing is not considered. During the algorithm development SVPWM it is assumed that the dc-link voltage is already balanced (e.g. by additional hardware).

The paper is organised as follows. The steps for developing the proposed SVPWM algorithm are presented in detail in Section 2. In Section 3, the method of how to implement the proposed algorithm is detailed, and obtained experimental results that prove the validity of the developed SVPWM algorithm are presented. The performance comparison between the proposed algorithm and carrier-based methods is also included. Finally, Section 4 concludes the work.

2. Space vector algorithm

The analysed drive topology is a standard three-level NPC inverter driving an asymmetrical six-phase induction machine, configured with a single neutral point, as shown in Fig. 1. This topology has $3^6 = 729$ switching states 0 to 728 which in normalised six-digit ternary numeral system are denoted as 000000 to 222222. Normalisation of the output leg voltages (v_{LEGk}) is done by $V_{dc}/2$.

Since an inverter is used to drive the machine, the attainment of sinusoidal phase voltage (v_{phk}) waveforms has to be done through the realisation of v_{LEGk}. The relationship between v_{phk} and v_{LEGk} can be defined as:

$$v_{phk} = v_{LEGk} - \frac{1}{6}\sum_{k=1}^{6} v_{LEGk} \qquad (1)$$

where $k = 1$ to 6, which also corresponds to phases a to f. The second term in (1) represents CMV, which is a scalar value. Hence, one can see from (1) that the order of v_{phk} waveforms is identical as the order of v_{LEGk} waveforms, at any instant of time. This indicates the possibility to realise

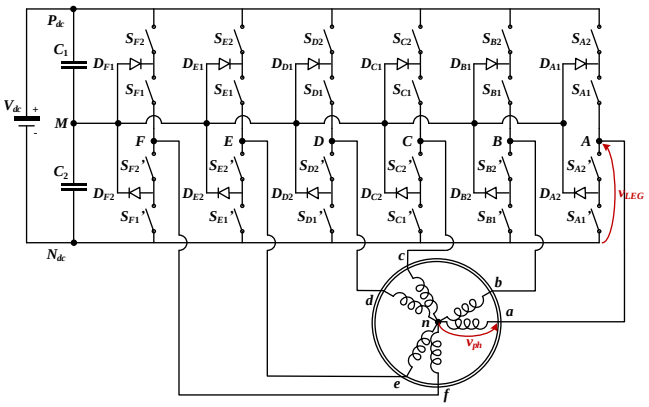

Fig. 1. *Circuit topology of analysed three-level asymmetrical six-phase drive.*

sinusoidal v_{phk} waveforms if v_{LEGk} are sinusoidal on average. In order to realise this, the inverter switches have to be controlled in a proper sequence, i.e. by choosing the correct set of switching states. In other words, the objective of the proposed SVPWM algorithm in this paper is to properly apply the switching sequences for certain duration of time such that the generated v_{LEGk} waveforms are sinusoidal on average, hence realising sinusoidal v_{phk} waveforms. The procedures for choosing the right switching sequences and calculating the dwell times are addressed in next sub-sections.

2.1. Three-level asymmetrical six-phase space vectors

The space vector projections for any set of variables (e.g. v_{phk} or v_{LEGk}) of asymmetrical six-phase drive can be obtained using VSD approach through transformation matrix:

$$\begin{bmatrix} v_\alpha \\ v_\beta \\ v_x \\ v_y \\ v_{0^+} \\ v_{0^-} \end{bmatrix} = \frac{2}{6} \cdot \begin{bmatrix} 1 & \cos(\alpha) & \cos(4\alpha) & \cos(5\alpha) & \cos(8\alpha) & \cos(9\alpha) \\ 0 & \sin(\alpha) & \sin(4\alpha) & \sin(5\alpha) & \sin(8\alpha) & \sin(9\alpha) \\ 1 & \cos(5\alpha) & \cos(8\alpha) & \cos(\alpha) & \cos(4\alpha) & \cos(9\alpha) \\ 0 & \sin(5\alpha) & \sin(8\alpha) & \sin(\alpha) & \sin(4\alpha) & \sin(9\alpha) \\ 1 & 0 & 1 & 0 & 1 & 0 \\ 0 & 1 & 0 & 1 & 0 & 1 \end{bmatrix} \cdot \begin{bmatrix} v_a \\ v_b \\ v_c \\ v_d \\ v_e \\ v_f \end{bmatrix} \qquad (2)$$

where $\alpha = \pi/6$. Substitution of 729 switching states into (2) results in 729 projection of v_{LEGk} space vectors into three orthogonal two-dimensional planes: α-β, x-y and 0^+-0^-. In other words, each switching state yields unique v_{LEGk} space vector. In addition, by substituting (1) into (2), the projection of v_{phk} space vectors onto those planes can be obtained in a similar way. The total number of v_{phk} space vectors is 665. Note that the number of v_{phk} space vectors is less than the number of switching states, which means that the redundancy is present.

One finds that the projections of v_{LEGk} and v_{phk} space vectors into α-β and x-y planes are identical, but they are different in 0^+-0^- plane. Furthermore, different low order harmonics map into each plane. The low order harmonics of the order $12k \pm 1$ ($k = 0, 1, 2, 3, \ldots$) of the v_{LEGk} or v_{phk} space vectors are mapped into α-β plane while the low order harmonics of the order $12k \pm 5$ ($k = 0, 1, 2, 3, \ldots$) and $3k$ ($k = 1, 3, 5, \ldots$) are mapped into x-y and 0^+-0^- planes, respectively [11]. The low order harmonics that map into α-β plane contribute to the machine's torque production. The low order harmonics that map into x-y and 0^+-0^- planes contribute only to the machine losses, hence their existence is undesirable. Therefore, the average voltage value in x-y and 0^+-0^- planes must be controlled to zero.

2.2. Reduction of the number of space vectors

Even though the total number of v_{phk} space vectors is large, not all of them can be chosen to achieve the desired sinusoidal v_{phk} waveforms. These v_{phk} space vectors can be identified by implementing order-per-sector law [10]. The order-per-sector law states that the projected v_{phk} space vectors in each sector in α-β plane (including the space vectors located on the borders of the bordering sectors, as well as at the origin) must satisfy the order of the sinusoidal reference phase voltage waveforms (v_{phk}^*), for the corresponding sector in time domain. The v_{phk}^* waveforms for asymmetrical six-phase system are defined as:

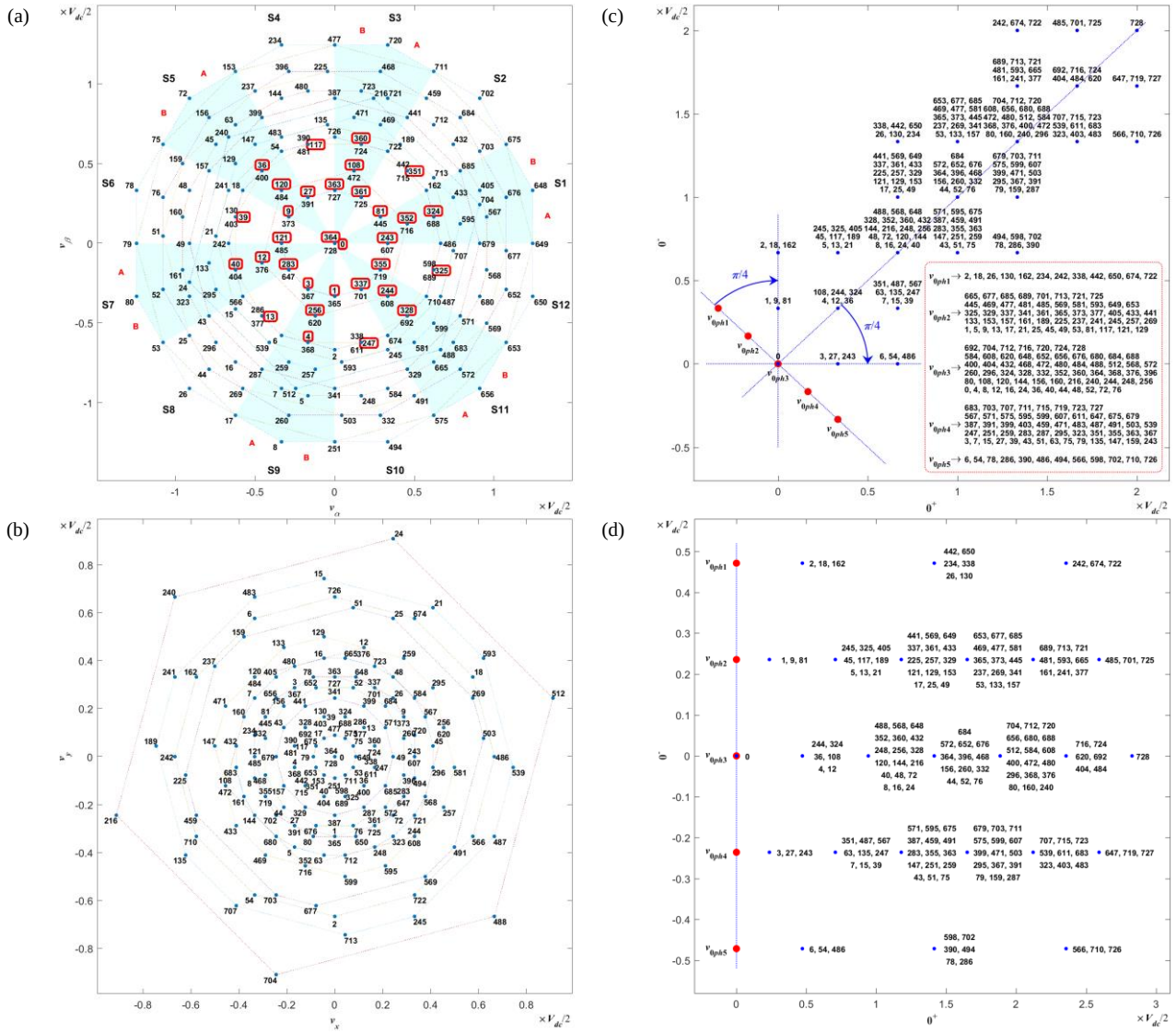

Fig. 2. *Projection of leg (in blue) and phase (in red) voltage space vectors (identical in α-β and x-y plane) of the analysed inverter after implementation of the order-per-sector law in the:* ***(a)*** *α-β* ***(b)*** *x-y* ***(c)*** 0^+-0^- *plane and* ***(d)*** 0^+-0^- *plane after rotational transformation for* $-\pi/4$.

$$v_{phk}^{*} = V^{*}\cos(\omega t - i \cdot \pi/6) \qquad (3)$$

where $k = a$ to f, while the corresponding values of i are $i = 0, 1, 4, 5, 8$ and 9. By plotting reference phase voltages of (3), one finds that v_{phk}^{*} reference values change their mutual order at 0°, 15°, 30°, 60° 75°, 90°, 150°, etc. These angles also correspond to the sector angles in α-β plane where the odd sectors are further sub-divided into two sections at 15° angle, while even sectors span the entire 30°.

As the projected v_{phk} and v_{LEGk} space vectors are identical in α-β plane, the order-per-sector law can be implemented by simply comparing the order of the normalised v_{LEGk} levels in the switching states (when represented in six-digit ternary numeral system) with the order of v_{phk}^{*} in the time domain. As a result, the numbers of v_{LEGk} and v_{phk} space vectors are significantly reduced, from 729 to 195 and from 665 to 163, respectively. The remaining v_{LEGk} and v_{phk} space vector projections in α-β, x-y and 0^+-0^- planes are shown in Fig. 2a to Fig. 2c. As already mentioned, the leg and phase voltage space vector projections in α-β and x-y plane are identical. This is not the case in 0^+-0^- plane; hence the projected v_{phk} space vectors in Fig. 2c are shown as red dots. They are denoted as v_{0ph1} to v_{0ph5}.

2.3. Rotational transformation of 0^+-0^- plane

Clearly, the projections of v_{phk} space vectors are along a straight line in the 0^+-0^- plane, which makes the analysed topology a five-dimensional system [11]; yet both 0^+ and 0^- axes are still dependent on each other. Therefore, in order to make it a genuine five-dimensional system, the components of one of the axes should always be zero. This can be achieved by rotating the projected v_{phk} space vectors and aligning them along 0^- axis, through a rotational transformation by $-\pi/4$, as illustrated in Fig. 2c. As a result, the transformation matrix of (2), can be redefined as:

$$\begin{bmatrix} v_\alpha \\ v_\beta \\ v_x \\ v_y \\ v_{0^+} \\ v_{0^-} \end{bmatrix} = \frac{2}{6} \cdot \begin{bmatrix} 1 & \cos(\alpha) & \cos(4\alpha) & \cos(5\alpha) & \cos(8\alpha) & \cos(9\alpha) \\ 0 & \sin(\alpha) & \sin(4\alpha) & \sin(5\alpha) & \sin(8\alpha) & \sin(9\alpha) \\ 1 & \cos(5\alpha) & \cos(8\alpha) & \cos(\alpha) & \cos(4\alpha) & \cos(9\alpha) \\ 0 & \sin(5\alpha) & \sin(8\alpha) & \sin(\alpha) & \sin(4\alpha) & \sin(9\alpha) \\ \frac{1}{\sqrt{2}} & \frac{1}{\sqrt{2}} & \frac{1}{\sqrt{2}} & \frac{1}{\sqrt{2}} & \frac{1}{\sqrt{2}} & \frac{1}{\sqrt{2}} \\ \frac{-1}{\sqrt{2}} & \frac{1}{\sqrt{2}} & \frac{-1}{\sqrt{2}} & \frac{1}{\sqrt{2}} & \frac{-1}{\sqrt{2}} & \frac{1}{\sqrt{2}} \end{bmatrix} \cdot \begin{bmatrix} v_a \\ v_b \\ v_c \\ v_d \\ v_e \\ v_f \end{bmatrix} \qquad (4)$$

It should be noted that the new rotational transformation of 0^+-0^- plane does not affect either the mapping of low order harmonics or the number of v_{LEGk} and v_{phk} space vectors, either before or after the order-per-sector law implementation.

The new projected v_{phk} and v_{LEGk} space vectors into 0^+-0^- plane are shown in Fig. 2d. Although the coefficients of $\pm 1/\sqrt{2}$ in 0^+ and 0^- axes in (4) are obviously due to the applied rotational transformation, the existence of these coefficients can also be analytically proven as a scaling factor for the amplitude of v_{phk} low order harmonics of the order $3k$ ($k = 1, 3, 5, \dots$) in terms of the amplitude of the corresponding v_{LEGk} low order harmonics [17]. Recall that these low order harmonics are mapped onto 0^+-0^- plane.

Moreover, one can also relate the projection of v_{LEGk} space vectors onto 0^+ axis to CMV [17]. Normally, in practice, CMV is not considered (i.e. it is not controlled) in space vector algorithms and this is the case also here. This makes the projection of v_{LEGk} and v_{phk} space vectors identical on all remaining considered axes: $\alpha, \beta, x, y, 0^-$. Therefore, it can be said that by not considering CMV, the determination of the switching sequences by means of selecting v_{LEGk} space vectors, i.e. corresponding switching states, will achieve the same realisation of v_{phk} waveforms.

From the control point of view, it is advantageous to implement (4) instead of (2) in developing the space vector algorithm for the analysed drive topology. Therefore, any reference made to 0^+-0^- plane henceforth in the paper will refer to 0^+-0^- plane after the implementation of rotational transformation, i.e. the plane shown in Fig. 2d.

2.4. Determination of potential switching sequences

With the aim of realising sinusoidal v_{phk} waveforms, the selection of v_{LEGk} space vectors and the corresponding switching states has to meet several general requirements and conditions. One of the main requirements is that the average value of x-y plane and 0^- axis components must be zero. This assumption has also been used in other VSD based multilevel multiphase algorithms [10-14]. Furthermore, in order to minimise switching losses and $\mathrm{d}v/\mathrm{d}t$, it is desirable that the v_{LEGk} levels only increase by one level per transition in the first half of the switching period and decrease by one level per transition in the second half [18]. This will results in having symmetrical PWM switching signals within a switching period. Since the transition of v_{LEGk} levels in the second half of the switching period is just the opposite of the first half, it is adequate to consider only the first half of switching period in the selection process of switching sequences.

On one hand, there are six v_{LEGk} level transitions in the first half of the switching period, which results in having seven switching states in each switching sequence. On the other hand, the number of chosen space vectors in each switching sequence must be equal to the number of machine phases [19], i.e. six in this case. This indicates that two of the chosen switching states in a switching sequence have identical space vector projections on all considered axes. In fact, these redundant switching states are the first, i.e. the starting, and the seventh switching state. Therefore, the selection of the starting switching states should also consider the existence of its redundant switching states. Furthermore, since each v_{LEGk} level increases by one level in each transition, the potential starting switching states can only contain 'zeros', 'ones' or combination of the two, for the analysed drive topology [12]. As a result, only 32 out of 195 remaining switching states (enclosed in the red boxes in Fig. 2a) satisfy the stated requirements and can be chosen as the starting switching states.

Based on the condition where each transition of the v_{LEGk} levels is increased by one, one can easily determine the subsequent switching states. Normally, their corresponding space vectors are projected into the same sector as the space vector of the starting switching states in the α-β plane [12-14]. Yet, for the analysed drive topology, this is not the case. Therefore, a new method, where all remaining switching states (regardless of their sector position) have to be considered as candidates for the subsequent switching state, needs to be implemented.

Since there are six v_{LEGk} transition levels in a switching sequence, there are 6! = 720 possible permutations of switching sequences per selected starting switching state. But, not all possible permutations can be considered as potential switching sequences since some of the switching sequences also comprise of switching states which have been previously eliminated by order-per-sector law. In other words, the number of potential switching sequences should be less than 720 per starting switching state. Due to immense number of potential switching sequences (combinations of switching states) that need to be considered, a permutation method has been developed in Matlab, to ease the selection process.

As an example, out of 720 permutations of switching sequence with starting switching state 324 (110000), only 102 can be considered as potential switching sequences. All possible single level v_{LEGk} transitions of these 102 potential switching sequences are illustrated with six different colours of arrows (each colour of arrows represents each inverter leg transition) as shown in Fig. 3. Only transitions in α-β plane are shown. These 102 potential switching sequences produce unique transition patterns in α-β, x-y and 0^+-0^- planes. However, it should be noted that due to numerous potential switching sequences that can be obtained from other starting switching states, there are higher possibilities among those potential switching sequences in having identical transition patterns, i.e. redundancy, in potential switching sequences.

By graphically analysing the transition patterns of the potential switching sequences [10], one finds that not all potential switching sequences can satisfy the requirement that the values of x-y and 0^+-0^- plane components can be zero on average. Thus, the number of potential switching sequences can be reduced further. As an example, for potential switching sequences with starting switching state 324, only 54 out of 102 satisfy the stated requirement. However, in order to completely determine the potential switching sequences for the analysed drive topology, this graphical method is still insufficient. Therefore, a method relying on numerical solutions is directly applied instead and this method will be addressed further in next sub-section.

Since the permutation method determines the potential switching sequences by taking into account all of the possible single level transitions of v_{LEGk} for each identified starting switching state, it is also valid for other drives with any number of inverter levels and machine phases.

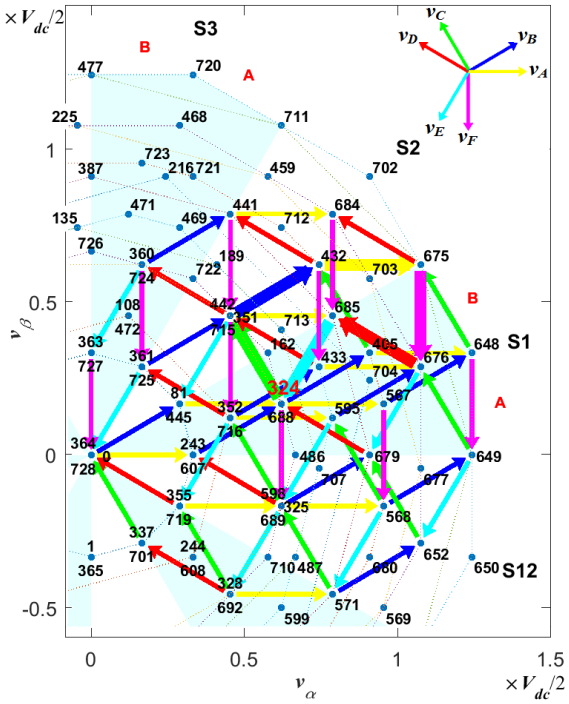

Fig. 3. *All possible single level increasing transitions of v_{LEGk} for starting switching state 324 (110000).*

2.5. Dwell time calculation and sector division

The dwell times typically refer to the duration of applied space vectors in any chosen switching sequence. Thus, the calculation of dwell times is based on space vector projections of the respective switching sequences. Hence, each transition pattern yields different value of dwell times and, consequently, the switching sequences which correspond to the same transition patterns will have the same value of dwell times [14]. The dwell times can be calculated using standard volt-second balance principle as well as time balancing equation which can be put in matrix form as:

$$\begin{bmatrix} T_1 \\ T_2 \\ T_3 \\ T_4 \\ T_5 \\ T_6 \end{bmatrix} = \begin{bmatrix} v_{\alpha,1} & v_{\alpha,2} & v_{\alpha,3} & v_{\alpha,4} & v_{\alpha,5} & v_{\alpha,6} \\ v_{\beta,1} & v_{\beta,2} & v_{\beta,3} & v_{\beta,4} & v_{\beta,5} & v_{\beta,6} \\ v_{x,1} & v_{x,2} & v_{x,3} & v_{x,4} & v_{x,5} & v_{x,6} \\ v_{y,1} & v_{y,2} & v_{y,3} & v_{y,4} & v_{y,5} & v_{y,6} \\ 1 & 1 & 1 & 1 & 1 & 1 \\ v_{0^-,1} & v_{0^-,2} & v_{0^-,3} & v_{0^-,4} & v_{0^-,5} & v_{0^-,6} \end{bmatrix}^{-1} \cdot \begin{bmatrix} v_\alpha^* \\ v_\beta^* \\ v_x^* \\ v_y^* \\ 1 \\ v_{0^-}^* \end{bmatrix} \cdot T_s \quad (5)$$

where T_k $(k = 1, 2, \dots, 6)$ are the dwell times of the applied space vectors.

The first four and the last row of the inverse matrix in (5) correspond to α, β, x, y, and 0^- projections of the six chosen space vectors in the switching sequence. Note that 0^+ axis (i.e. the fifth row) is omitted in (5), as it represents CMV, and is replaced with the time balancing equation which ensures that the sum of calculated dwell times is equal to the switching period, T_s. In addition, since the first and seventh switching state correspond to the same space vector, it is desirable for its calculated dwell time i.e. T_1 to be equally shared between the two [20]. The reference voltages of α and β axes in (5) i.e. v_α^*, and v_β^* are set to $V^* \cdot \cos(\omega t)$, and $V^* \cdot \sin(\omega t)$, respectively while the references for x, y and 0^- axes, i.e. v_x^*, v_y^* and v_0^*-, are set to zero. The references are set as such because they are equivalent to representation of sinusoidal v_{phk}^* waveforms in those three axes. In other words, by substituting (3) into (4), one finds that the projected v_{phk}^* space vector has a radius of V^* and travels at angular speed of ω which forms a circular trajectory in α-β plane but stays at the origin, i.e. zero, in x-y and 0^+-0^- planes. Note that if a multi-frequency output, with a-priori known value of the reference in the x-y plane, is desired it can be obtained by setting v_x^* and v_y^* to the adequate non-zero reference values. However, note that this will have a consequence on all calculations hereafter. Therefore, it is important to emphasise that the algorithm is presented for sinusoidal references (as is the case in [10-14]), and is not aimed for multi-frequency operation.

Furthermore, one finds that the solutions for the dwell time calculations of some transition patterns only exist in certain regions of the α-β plane. These regions are commonly known as regions of application and can be identified either using analytical calculation [10] or by visualisation of numerical solutions of (5) in the α-β plane [14]. The regions of applications are separated by sector borders. Solving the problem analytically becomes more involved if the number of phases is increased and if asymmetrical machine is considered. Hence, in this paper, the latter method is adapted. However, it is fair to say that once the sector borders are determined it is it is irrelevant if they were calculated analytically or numerically. The visualisation of used numerical solutions is representation of consecutive dots where the dots indicate the locations of the applied v_α^* and v_β^*, if the solution of (5) does exist. In essence, while gradually increasing the magnitude of v_α^* and v_β^* (V^*) from zero to $0.644 \cdot V_{dc}$ (from the origin until the circumradius of the largest polygon in α-β plane), the dwell times of each transition pattern are repetitively calculated with the help of Matlab code. If the solution for dwell times exists, a dot is plotted at the current values of v_α^* and v_β^*. As an example, transition pattern denoted by the thick arrows in Fig. 3, which corresponds to switching sequence 110000-111000-121000-221000-221001-221101-221111, produces a region of application illustrated by different coloured dots in Fig. 4.

One finds that only 40 out of 102 potential switching sequences, i.e. transition patterns, obtained from starting switching state 324, have a solution for dwell times calculation. This proves the inadequacy of graphical method in completely determining the switching sequences (where the reduction was done to 54 sequences). Besides, those 40 switching sequences also form 40 unique regions of application, as shown in Fig. 4 (denoted by 1 to 40), and divide the sectors into several geometrical shapes. Hence, the regions of application also represent sub-sectors. The regions of application also correspond to potential switching sequences obtained from other starting switching states. Regions of application for starting switching state 351 (111000) can also be identified in a similar way, and are also shown in Fig. 4 (denoted by 1 to 31 in red colour). It can be seen that several regions of application can be associated to potential switching sequences either with starting switching state 324 or 351. Since the existence of regions of application is unique to transition patterns, this indicates switching sequences which yield identical transition patterns in α-β, x-y and 0^+-0^- planes, thus confirming the existence of potential switching sequence redundancies.

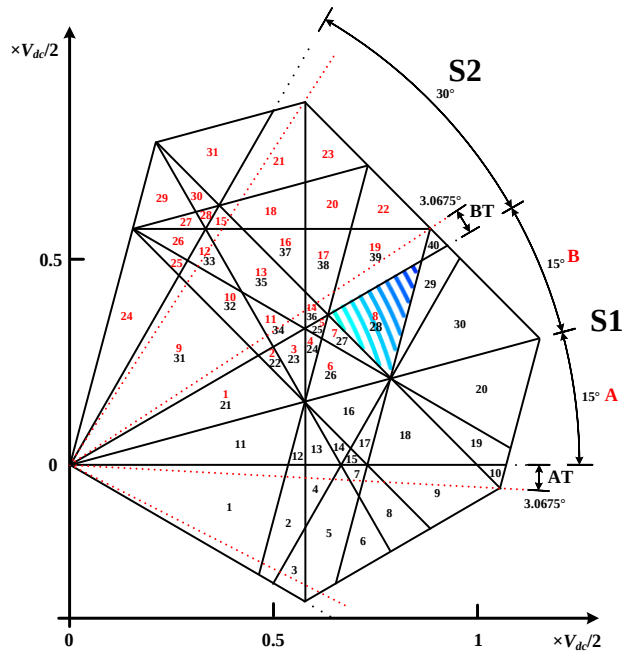

Fig. 4. *Regions of application of all possible transition patterns for starting switching states 324 (110000) and 351 (111000).*

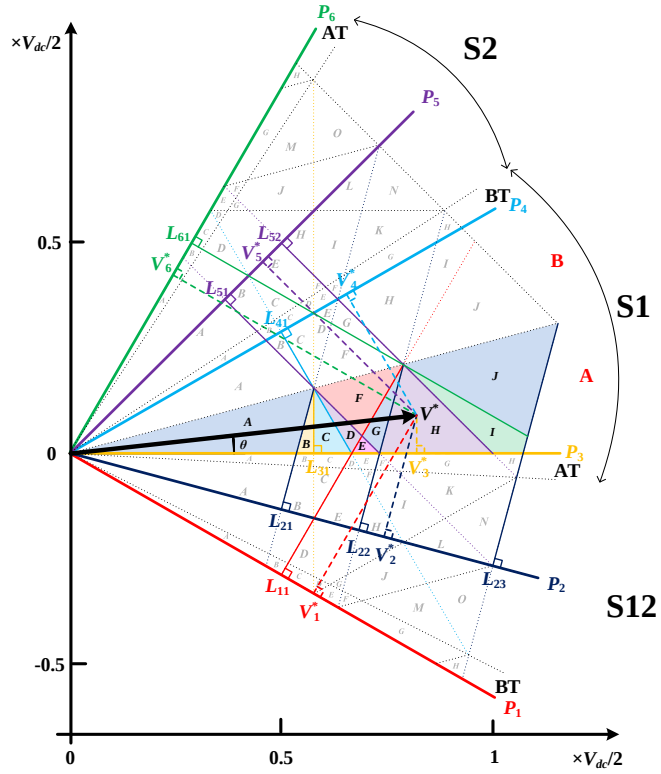

Fig. 5. *Sub-sector determination based on the location of the projected v^*_{phk} space vector in S1-A.*

2.6. Potential switching sequence optimisation

The existence of potential switching sequence redundancies gives more freedom in the process of the switching sequence optimisation. The optimisation process is actually based on minimisation of the switching losses, where the switching sequences of the all sub-sectors within a sector should belong to the same starting switching state [20]. Thus, during the transition between sub-sectors, additional switching losses can be avoided. However, in Fig. 4, sub-sectors 10 and 40 of starting switching state 324 are located outside the first sector (S1) and it can be shown that they also do not have any redundant potential switching sequences. Therefore, in order to meet the stated requirement, two additional small sectors, each consisting of eight sub-sectors, are introduced at each side of odd sectors (denoted by AT and BT in Fig. 4). Because of this, one can say that each odd sector is actually comprised of A, AT, B and BT sectors.

At this stage (when the process of optimisation is completed), the switching sequences as well as the sub-sectors for all sectors, have been completely determined. As an example, the switching sequences of the first section of the first sector (S1-A) are listed in Table 1, and their corresponding sub-sectors are shown in Fig. 5. Note that only the switching states in the first half of the switching period are listed in Table 1, since the order of the switching states is reversed in the second half.

Table 1. Selected switching sequences for S1-A.

Sub-sector	Selected switching sequence
A	110000-110001-111001-111011-111111-211111-221111
B	110000-110001-111001-111011-211011-211111-221111
C	110000-110001-111001-111011-211011-221011-221111
D	110000-110001-111001-211001-211011-221011-221111
E	110000-110001-210001-211001-211011-221011-221111
F	110000-110001-111001-211001-221001-221011-221111
G	110000-110001-210001-211001-221001-221011-221111
H	110000-110001-210001-220001-221001-221011-221111
I	110000-210000-210001-220001-221001-221011-221111
J	110000-210000-220000-220001-221001-221011-221111

2.7. Sub-sector determination

It has been shown that the chosen switching sequences and their corresponding dwell times are highly dependent on the location of projected v^*_{phk} space vector in α-β plane. But, in time, the projected v^*_{phk} space vector travels along a circular trajectory and passes through the sectors as well as sub-sectors. Hence, the corresponding switching sequences and calculated dwell times have to be applied accordingly. In order to accommodate this, a method introduced in [10] where the borders of the sub-sectors are utilised to determine the current location of the projected v^*_{phk} space vector in the α-β plane is adopted. An illustration on how this method is applied for S1-A is shown in Fig. 5.

There are nine borders between the sub-sectors of S1-A, these borders can be projected onto six axes P1 to P6, which are perpendicular to borders. Because numerical method was used, a careful visual analysis of the regions of application and sector borders has been done. It is concluded that the borders between sectors are straight lines (see Fig. 4). This was confirmed in Matlab by setting even smaller step for V^* and θ (where $\theta = \omega t$) then the one used for generation of Fig. 4. The distances from the intersection points between the projected borders and axes P1 to P6, with respect to the origin, also referred to as limits and denoted as L_{11}, L_{21}, L_{22}, …, L_{61}, are calculated using simple trigonometry and the values of the angles at which borders are located. To convert irrational numerical values (obtained from Matlab code) to standard

Table 2. Conditions defining the sub-sectors that correspond to the location of the v^*_{phk} space vector in S1-A.

Sub-sector	Conditions0 $\leq \theta <$ 15°: and	where:
A	$V_2^* \leq L_1$	$V_1^* = V^* \cos(\omega t + \pi/6)$
B	$V_2^* > L_1,\ V_3^* \leq L_2$	$V_2^* = V^* \cos(\omega t + \pi/12)$
C	$V_3^* > L_2,\ V_4^* \leq L_2$	$V_3^* = V^* \cos(\omega t)$
D	$V_4^* > L_2,\ V_5^* \leq L_1,\ V_1^* \leq L_2$	$V_4^* = V^* \cos(\omega t - \pi/6)$
E	$V_1^* > L_2,\ V_5^* \leq L_1$	$V_5^* = V^* \cos(\omega t - \pi/4)$
F	$V_5^* > L_1,\ V_1^* \leq L_2$	$V_6^* = V^* \cos(\omega t - \pi/3)$
G	$V_1^* > L_2,\ V_5^* > L_1,\ V_2^* \leq L_3$	
H	$V_2^* > L_3,\ V_5^* \leq L_3$	
I	$V_5^* > L_3,\ V_6^* \leq L_2,\ V_2^* \leq L_4$	
J	$V_6^* > L_2,\ V_2^* \leq L_4$	

mathematical representation, the fact that L_{23} corresponds to the maximum linear modulation index value of 1.035 [which also can be written as $\sqrt{2} \cdot (\sqrt{3} - 1)$], was used. Based on it one can find that: $L_{21} = L_{51} = \sqrt{2} \cdot (\sqrt{3} - 1)/4 \cdot V_{dc}$, $L_{11} = L_{31} = L_{41} = L_{61} = \sqrt{3}/6 \cdot V_{dc}$, $L_{22} = L_{52} = \sqrt{2}/4 \cdot V_{dc}$ and $L_{23} = \sqrt{2} \cdot (\sqrt{3} - 1)/2 \cdot V_{dc}$. These four limits are denoted further with L_1, L_2, L_3 and L_4, respectively. Similarly, the α-β component of v^*_{phk} space vector can also be projected onto the same perpendicular axes i.e. P_1 to P_6. The distances between the point of intersections between the two to the origin (denoted as V_1^* to V_6^*) are calculated and then compared to those limits. As a result, the current location of projected v^*_{phk} space vector can be accurately determined at any given time instant, hence the correct switching sequence and corresponding dwell times can also be applied accordingly. The required conditions in determining the sub-sectors for S1-A are listed in Table 2. To understand the process of determination of the sub-sector in which the reference is located careful analysis of the conditions in Table 2 and graphical visualisation of those conditions in Fig. 5 is mandatory. Finally, it should be noted that when this method is applied to the other sectors (e.g. S1-B, S1-AT etc.), the projections of the sub-sectors' borders onto their respective perpendicular axes (i.e. limits) might be different than those shown in Fig. 5. Therefore, although the previous four limits are also applicable to other sectors, one has to identify and denote the relevant limits as well as the required conditions accordingly.

3. Experimental results

Despite the complex selection process presented in Section 2, the real implementation of the presented SVPWM algorithm is actually rather simple. In fact, only the relevant switching sequence (chosen based on the current location of v^*_{phk} space vector projections in the α-β plane) and its corresponding dwell times are required in order to generate the switching signals for the inverter switches. Recall that all switching sequences have already been determined offline in Section 2. For these switching sequences, the corresponding inverse matrices (as in (5)) for dwell time calculation can also be pre-calculated and stored as constants in the memory. In addition, the total number of saved switching sequences and pre-calculated inverse matrices can be reduced further by implementing sector pair relation [13] and mapping the other sectors onto the first three sectors S1 to S3. Although the

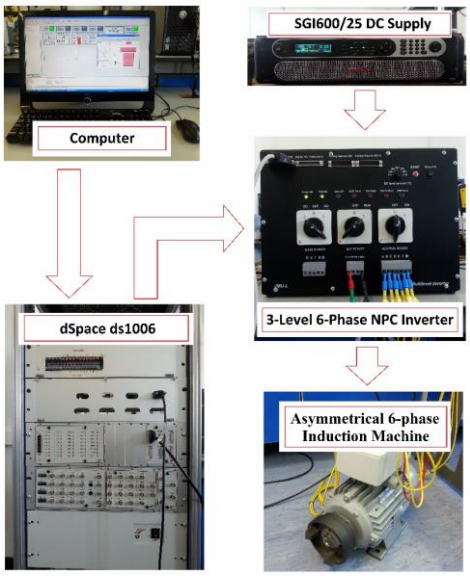

Fig. 6. *Experimental setup.*

denotation of sub-sectors in S3 is identical to S1, it is difficult to obtain a simple implementation of relationship between these two sectors. This is so since the compositions of v_{LEGk} levels of the switching states in S3 switching sequences are different than in S1. Also, it should be noted that even sectors S4, S8 and S12 are mirrored compared to S2, S6 and S10. Thus, the obtained switching sequences for S4, S8 and S12, when mapped into S2, have to be rearranged and the corresponding dwell times calculated accordingly.

In summary, the implementation of the proposed SVPWM algorithm is simply done by accurately determining the current location of the applied v^*_{phk} in α-β plane. The corresponding sector is then mapped into the first three-sectors (S1 to S3). Next, the respective switching sequence and pre-calculated inverse matrix are fetched from the memory. After that, the corresponding switching sequence is generated based on the sector mapping relation while the dwell times are calculated using the pre-calculated inverse matrix. A simple rearrangement of generated switching sequences and calculated dwell times should be applied accordingly for even sectors. Finally, the application of obtained switching sequence and calculated dwell times generates the switching signals for the inverter switches.

A PWM modulator, based on the introduced SVPWM algorithm, is developed and programmed into a real-time platform (dSpace ds1006) through Matlab/Simulink. The experimental setup is shown in Fig. 6. The V_{dc} is set to be 300 V using Sorensen SGI 600/25 external dc supply. The asymmetrical six-phase induction machine is operated under no-load condition and driven using a custom made three-level six-phase NPC inverter, which switches at $f_{sw} = 2$ kHz. The inverter dead time is 6 µs and it is not compensated. The machine's parameters are listed in Table 3. The SVPWM algorithm is tested in open loop for full linear range of modulation index (m_i) i.e. from 0.1 to 1.035, with 0.05 increment, using V/f control. The m_i is defined as:

$$m_i = V^*/(V_{dc}/2) \tag{6}$$

The peak voltage of v^*_{phk}, i.e. V^*, is chosen as 150 V at 50 Hz, which is the machine's rated frequency, and, according to (6), it corresponds to $m_i = 1$.

Table 3. Asymmetrical six-phase induction machine parameters.

Parameters	Value	
Resistance	R_s = 13.75 Ω	R_r = 5.775 Ω
Leakage inductance	L_{ls} = 5.3 mH	L_{lr} = 12.7 mH
Mutual inductance	L_m = 296.5 mH	

Although the main aim of this paper is in fact development and implementation of the new SVPWM algorithm, for comprehensiveness the presented algorithm is also compared with two commonly found carrier-based PWM (CBPWM) algorithms and one lesser-known algorithm. Considered algorithms are all with in-phase disposition of the carriers, while the references are pure sinusoidal (PD-SPWM), with min-max injection (PD-MM) and with double min-max injection (PD-DI). Details regarding the theory and implementation of PD-DI CBPWM for multilevel converters can be found in [21]. The performance of all modulation techniques is determined by means of total harmonic distortion (THD). The THD for the phase voltage (THD_v) and current (THD_i) are calculated using:

$$\mathrm{THD}_v = \sqrt{\sum_{k=2}^{h} V_k^2/V_1^2} \qquad \mathrm{THD}_i = \sqrt{\sum_{k=2}^{h} I_k^2/I_1^2} \qquad (7)$$

where V_k and I_k represent the k-th components of voltage and current in the spectrum, while V_1 and I_1 are the fundamental values of phase voltage and current, respectively. It should be noted that the first h harmonics, up to value of h that corresponds to 21 kHz, i.e. the first ten sidebands, are included in voltage and current THD calculations. The value of h is not fixed and depends on the value of the fundamental frequency, f. If the value of h was fixed then for low values of f switching harmonics may not be taken into equation (or just first few side-bands would be considered) and the calculated value of THD would be significantly reduced. On the other hand, selected way for THD calculation is more fair and is much more accurate.

The simulations for all modulators were done in PLECS software where the machine is modelled based on [24]. The results prove that the presented SVPWM and PD-DI, from the perspective of current THD, outperform the other modulation methods (Fig. 7). Furthermore, the results show that SVPWM and PD-DI methods have identical performances. Therefore, the investigation of SVPWM and PD-DI is taken further for the experimental comparison.

The measured phase 'a' leg voltage (v_A), phase voltage (v_a) and current (i_a) waveforms and corresponding spectra when $m_i = 0.4$ and $m_i = 1$ for the proposed algorithm as well as PD-DI, are shown in Fig. 8 and Fig. 9, respectively. One can see that the waveforms yielded by both modulation techniques are practically the same. Also, the values of the measured fundamental phase voltage are approximately the same as the reference values of V^* which are obtained from (6), i.e. 60 V and 150 V for $m_i = 0.4$ and 1, respectively. Further, although the v_x^*, v_y^* and v_0^*– are set to zero in the proposed algorithm to ensure that the low order harmonics of the order $12k \pm 5$ ($k = 0, 1, 2, 3, \ldots$) and $3k$ ($k = 1, 3, 5, \ldots$) do not exist, they are still present in both phase voltage and current spectra (see Fig. 8c and d and Fig. 9c and d), but are relatively small in magnitude. It can be shown (e.g. by simple simulation comparison without and with dead-time) that the appearance of these low odd order

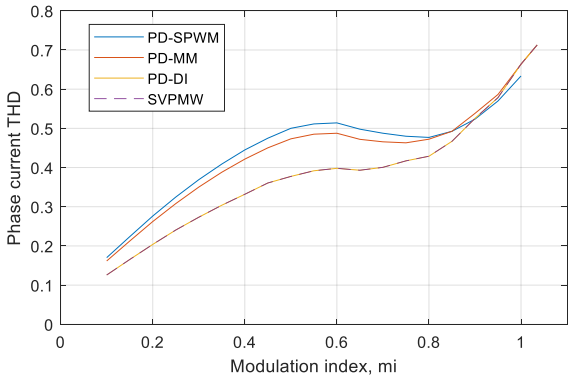

Fig. 7. *Comparison of calculated* $\mathbf{THD}_i$ *based on simulation results with an ideal inverter for full linear range of* $\boldsymbol{m_i} = \mathbf{0.1}$ *to* $\mathbf{1.035}$.

harmonics is purely the consequences of uncompensated inverter dead time [23].

The phase 'a' THD_v and THD_i obtained from the simulation and experimental results of the SVPWM algorithm and PD-DI modulator for full linear range of m_i are shown in Fig. 10 and Fig. 11, respectively. One can see that the THD_v and THD_i, obtained experimentally for both PWM techniques, are identical. It can be also observed that the THD characteristics, obtained by simulation and experimentally, are in very good agreement, with rather small differences. Since THD is normally used in practice as a figure of merit for measuring the performance of a modulation technique [24], it can be said that the proposed SVPWM algorithm and PD-DI for the analysed drive topology are proven to have identical performance, thus further validating the presented SVPWM algorithm.

As already mentioned, the variation of mid-point dc-link voltage is a common concern for NPC topology, but it is not actively controlled by the presented algorithm. To test the influence of the modulation method onto the dc-link mid-point voltage, the modulation index was changed in a step manner (i.e. as a square-wave at 2 Hz), between $m_i = 0.4$ to 1.0. Used converter has a total dc-link capacitance of 1.5 mF. The results shown in Fig. 12 prove that the proposed SVPWM algorithm is able to maintain the mid-point voltage stable at 150 V. Note that the transition is done in open loop using $V/f = \text{constant}$ law. Further analysis of the influence of the presented method onto variation of the dc-link mid-point voltage, e.g. using closed loop control such as field oriented control, is beyond the scope of this paper.

The complexity of the two algorithms has been compared as well. The execution time was measured using dSpace Profiler Tool. Execution time of the carrier-based PD-DI algorithm is 1.16 µs, while for the space vector algorithm it is 6.82 µs. It should be emphasised however that the execution time of the presented algorithm has been significantly reduced by storing significant amount of data in the memory. In the current implementation $71 \cdot 36 = 2556$ integer values for the switching sequences and 2556 double values for the corresponding pre-calculated inverse matrices of (5), for all sub-sectors within S1 to S3 were stored in the memory. Therefore, the memory usage of the presented algorithm is significantly higher than for PD-DI algorithm (which is an expected outcome when comparison of any two carrier-based and space vector algorithms is undertaken). Used implementation is acceptable for powerful platforms

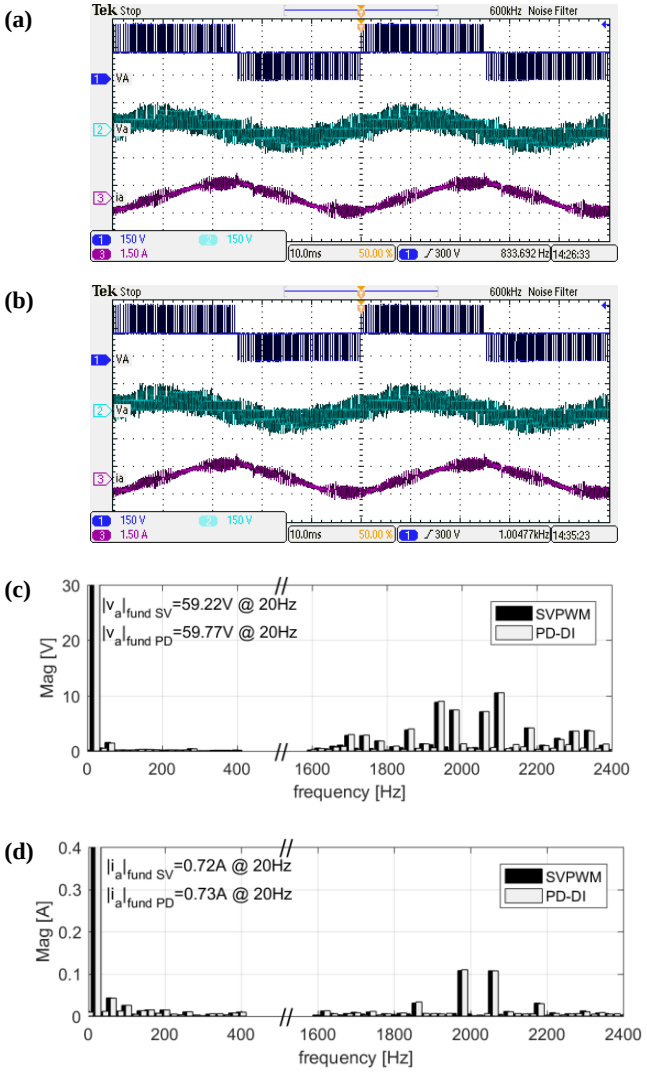

Fig. 8. *Oscilloscope capture of $\boldsymbol{v_A}$, $\boldsymbol{v_a}$ and $\boldsymbol{i_a}$ at $\boldsymbol{m_i = 0.4}$ for **(a)** developed SVPWM algorithm, **(b)** PD-DI, with corresponding **(c)** voltage and **(d)** current spectra (note: x-axis is segmented, to show important harmonics only).*

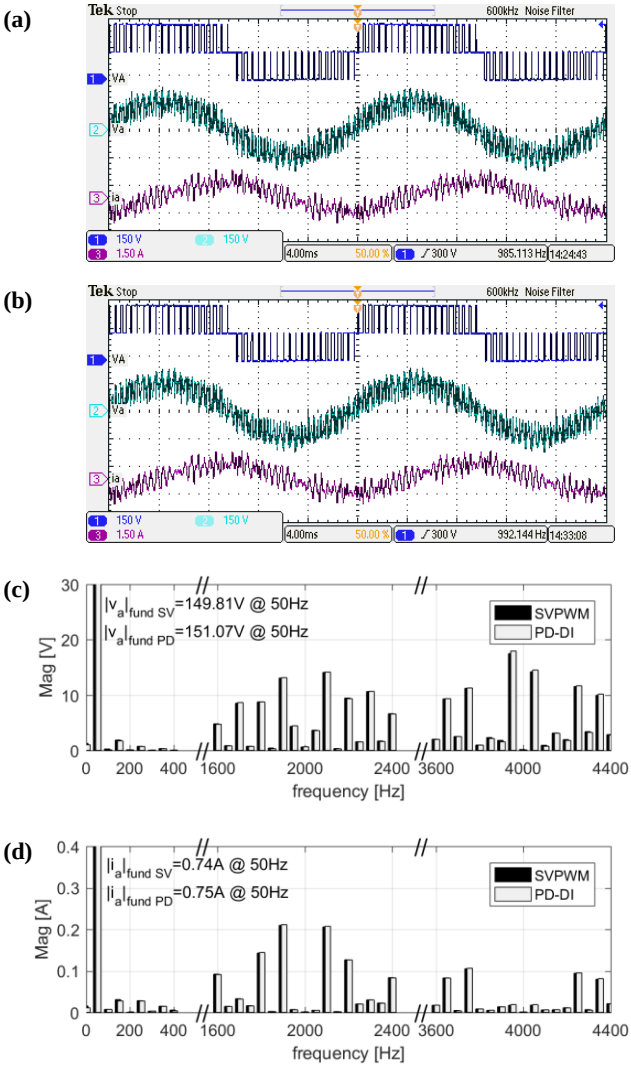

Fig. 9. *Oscilloscope capture of $\boldsymbol{v_A}$, $\boldsymbol{v_a}$ and $\boldsymbol{i_a}$ at $\boldsymbol{m_i = 1}$ for **(a)** developed SVPWM algorithm, **(b)** PD-DI, with corresponding **(c)** voltage and **(d)** current spectra (note: x-axis is segmented, to keep important harmonics only).*

with plenty of memory such as dSpace. However, it may be too demanding for lots of the standard microprocessors.

Regardless of the fact that the carrier-based and SVPWM based algorithms yield the identical performance (and mentioned drawbacks about multi-frequency operation, and dc-link voltage balancing), SVPWM algorithms should still be investigated, since they provide better insight and easier understanding of some the multiphase machine/system features (e.g. harmonic mapping – which has important consequences in control, possibilities for current and power sharing, post-fault operation, on-board battery chargers, multi-motor drives etc.). These are sometimes hard, or even impossible, to analyse from the carrier-based PWM perspective. Therefore, the results presented in this paper may be of significance to those researchers that use SVPWM and vector space decomposition when investigating new control possibilities for multiphase machines. Furthermore, this work proves, for the first time, that for practical implementation the same level of performance can be achieved using the easier to implement carrier-based PD-DI method.

Finally, the following should be noted. The algorithm is developed based on general principles of SVPWM algorithms for symmetrical multiphase three-level systems as in [10, 12-14]. However, because of the machine's asymmetry, one can see that some additional steps were required in the developed algorithm. These steps are for the first time developed and applied in this paper and are done in a general way so that may be used for the other cases as well. The additional steps are as follow. The additional rotational transformation is introduced in 0^+-0^- plane, to reduce the system to five-dimensional case. Further, the space vectors that should be selected to properly generate a reference located within a certain sector, now are not necessarily located within that sector. Therefore, general permutation method was introduced to solve this problem. Also, additional small sectors were introduced, to properly deal with the switching sequence redundancies and minimise the switching losses.

4. Conclusion

In this paper, a space vector algorithm based on VSD approach for three-level asymmetrical six-phase drive with single neutral point configuration is proposed and

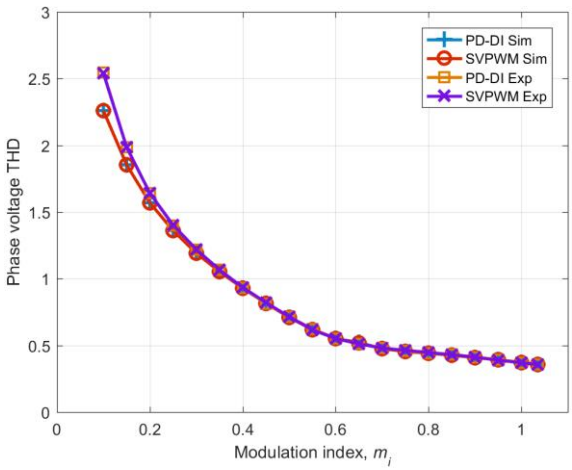

Fig. 10. *Comparison of calculated* $\mathbf{THD}_v$ *based on simulation and experimental results for the developed SVPWM algorithm and PD-DI for full linear range of* $\boldsymbol{m_i} = \mathbf{0.1}$ *to* $\mathbf{1}$.

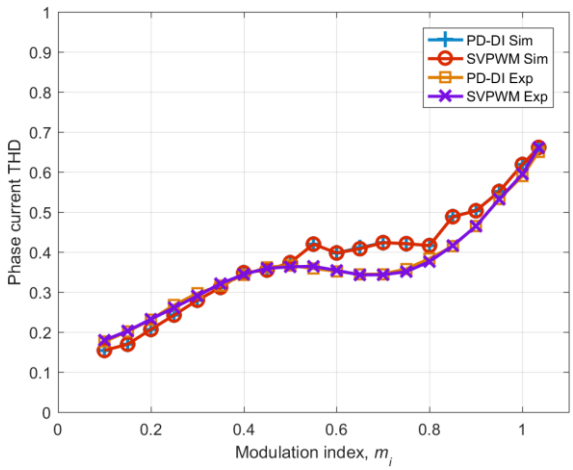

Fig. 11. *Comparison of calculated* $\mathbf{THD}_i$ *based on simulation and experimental results for the developed SVPWM algorithm and PD-DI for full linear range of* $\boldsymbol{m_i} = \mathbf{0.1}$ *to* $\mathbf{1}$.

experimentally tested for the first time. The required steps for developing the algorithm are presented in detail. A rotational transformation is applied to the 0^+-0^- plane in order to make the realisation of phase voltage waveforms possible through the leg voltage space vectors. In this way the problem is reduced to a five-dimensional case. The switching sequences are chosen by taking into account all possible single level leg voltage transitions by means of the introduced permutation method. Finally, the chosen switching sequences are applied according to the current location of the reference phase voltage space vector in the α-β plane. The proposed algorithm is validated through simulations and experiments, proving that the adequate value of the fundamental is obtained. The low order harmonics in the phase voltage and current spectra are present due to the uncompensated inverter dead time. Finally, the proposed SVPWM algorithm is compared with other CBPWM methods. It is shown that it obtains identical performance as PD-DI.

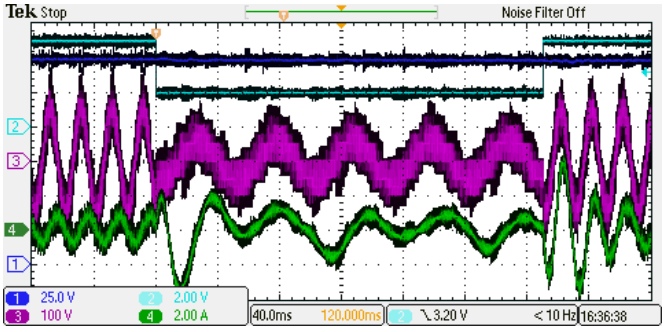

Fig. 12. *The impact of SVPWM on the dc-link mid-point voltage.* CH1 *midpoint voltage (dark blue);* CH2 *modulation index (cyan,* $\mathbf{5\ V}$ *corresponds to* $\boldsymbol{m_i} = \mathbf{1}$*);* CH3 *phase '*$\boldsymbol{a}$*' voltage (purple); and* CH4 *phase '*$\boldsymbol{a}$*' current (green).*

5. References

[1] E. Levi, "Advances in converter control and innovative exploitation of additional degrees of freedom for multiphase machines," *IEEE Trans. Ind. Electron.*, vol. 63, pp. 433-448, Jan 2016.

[2] H. S. Che, M. J. Duran, E. Levi, M. Jones, H. Wooi-Ping, and N. Abd Rahim, "Postfault operation of an asymmetrical six-phase induction machine with single and two isolated neutral points," *IEEE Trans. Power Electron.*, vol. 29, pp. 5406-5416, Oct 2014.

[3] E. Levi, F. Barrero, and M. J. Duran, "Multiphase machines and drives - Revisited," *IEEE Trans. Ind. Electron.*, vol. 63, pp. 429-432, Jan 2016.

[4] R. Bojoi, F. Farina, F. Profumo, and A. Tenconi, "Dual-three phase induction machine drives control - a survey," *IEEJ Trans. Ind. Appl.*, vol. 126, pp. 420-429, Jan 2006.

[5] A. Nabae, I. Takahashi, and H. Akagi, "A new neutral-point-clamped PWM inverter," *IEEE Trans. Ind. Appl.*, vol. 17, pp. 518-523, Sep 1981.

[6] G. Carrara, S. Gardella, M. Marchesoni, R. Salutari, and G. Sciutto, "A new multilevel PWM method: A theoretical analysis," *IEEE Trans. Power Electron.*, vol. 7, pp. 497-505, Jul 1992.

[7] Y.-H. Lee, D.-H. Kim, and D.-S. Hyun, "Carrier based SVPWM method for multi-level system with reduced HDF [harmonic distortion factor]," in *Proc. IEEE Ind. Appl. Soc. Annu. Meeting* (*IAS*), Rome, Italy, 2000, pp. 1996-2003.

[8] Fei Wang, "Sine-triangle versus space-vector modulation for three-level PWM voltage-source inverters," *IEEE Trans. Ind. Appl.*, vol. 38, pp. 500-506, Mar-Apr 2002.

[9] B. P. McGrath, D. G. Holmes and T. Lipo, "Optimized space vector switching sequences for multilevel inverters," *IEEE Trans. Power Electron*, vol. 18, pp. 1293-1301, Nov. 2003.

[10] L. Gao and J. E. Fletcher, "A space vector switching strategy for three-level five-phase inverter drives," *IEEE Trans. Ind. Electron.*, vol. 57, pp. 2332-2343, Jul 2010.

[11] Y. Zhao and T. A. Lipo, "Space vector PWM control of dual three-phase induction machine using vector space decomposition," *IEEE Trans. Ind. Appl.*, vol. 31, pp. 1100-1109, Sep 1995.

[12] O. Dordevic, M. Jones, and E. Levi, "A comparison of carrier-based and space vector PWM techniques for three-level five-phase voltage source inverters," *IEEE Trans. Ind. Informat.*, vol. 9, pp. 609-619, May 2013.

[13] E. A. R. Engku Ariff, O. Dordevic, and M. Jones, "A space vector PWM technique for a three-level symmetrical six phase drive," *IEEE Trans. Ind. Electron*., vol. 64, pp. 8396-8405, Nov. 2017.

[14] O. Dordevic, E. Levi, and M. Jones, "A vector space decomposition based space vector PWM algorithm for a three-level seven-phase voltage source inverter," *IEEE Trans. Power Electron.,* vol. 28, pp. 637-649, Feb 2013.

[15] C. Wang and Y. Li, "Analysis and calculation of zero-sequence voltage considering neutral-point potential balancing in three-level npc converters," *IEEE Trans. Ind. Electron.*, vol. 57, no. 7, pp. 2262-2271, July 2010.

[16] I. López et al., "Modulation strategy for multiphase neutral-point-clamped converters," *IEEE Trans. Power Electron.*, vol. 31, no. 2, pp. 928-941, Feb. 2016

[17] I. Zoric, M. Jones, and E. Levi, "Phase voltage harmonic imbalance in asymmetrical multiphase machines with single neutral point," in *Proc. IEEE Ind. Electron. Soc. Annu. Meeting* (*IECON*), Florence, Italy, 2016, pp. 4343-4348.

[18] H. W. van der Broeck, H. C. Skudelny, and G. V. Stanke, "Analysis and realization of a pulsewidth modulator based on voltage space vectors," *IEEE Trans. on Ind. Appl.,* vol. 24, pp. 142-150, Jan 1988.

[19] J. W. Kelly, E. G. Strangas, and J. M. Miller, "Multiphase space vector pulse width modulation," *IEEE Trans. Energy Conv.,* vol. 18, pp. 259-264, Jun 2003.

[20] B. P. McGrath, D. G. Holmes, and T. A. Lipo, "Optimized space vector switching sequences for multilevel inverters," *IEEE Trans. Power Electron.*, vol. 18, pp. 1293-1301, Nov 2003.

[21] G. Grandi and J. Loncarski, "Simplified implementation of optimised carrier-based PWM in three-level inverters," *IET Electronics Letters*, vol. 50, no. 8, pp. 631-633, Apr 2014.

[22] H. S. Che, A. S. Abdel-Khalik, O. Dordevic, and E. Levi, "Parameter estimation of asymmetrical six-phase induction machines using modified standard tests," *IEEE Trans. Ind. Electron.*, vol. 64, pp. 6075-6085, Aug. 2017.

[23] G. Grandi and J. Loncarski, "Analysis of dead-time effects in multi-phase voltage source inverters," in *Proc. IET Int. Conf. on Power Electron., Machines and Drives (PEMD)*, Bristol, U.K., 2012, pp. 1-6.

[24] O. Dordevic, M. Jones, and E. Levi, "Analytical formulas for phase voltage RMS squared and THD in PWM multiphase systems," *IEEE Trans. Power Electron.,* vol. 30, pp. 1645-1656, Mar 2015.